Chapter 2
Nb_3Sn Wires and Cables for High-Field Accelerator Magnets

Emanuela Barzi and Alexander V. Zlobin

Abstract Since the discovery of superconducting Nb_3Sn in 1954, continuous developments have led to a strong improvement of its properties. This chapter describes the evolution of Nb_3Sn fabrication techniques since the 1960s and the main properties of modern Nb_3Sn composite wires and Rutherford cables.

2.1 Introduction

The intermetallic compound Nb_3Sn, discovered by Matthias et al. (1954), is a type II superconductor having a stoichiometric composition ranging from 18–25 atomic percent (at. %) Sn. Its crystal structure is classified as A15 (also known as β-tungsten). The critical temperature T_{c0} is ~18 K, and the upper critical magnetic field B_{c20} can reach 30 T. As a comparison, the ductile alloy Nb-Ti has a T_{c0} of 9.8 K and a B_{c20} of 14.5 T, which makes Nb-Ti adequate only for operational magnetic fields of up to 8–9 T. Thanks to its larger critical current density J_c, Nb_3Sn enables operating fields in accelerator magnets above 10 T. This field is larger than any achieved with present Nb-Ti particle accelerator magnets. Some of the challenges with Nb_3Sn are that it requires high-temperature processing to create the superconducting Nb_3Sn phase. It is also a brittle material, which makes it strain-sensitive, i.e., high strain on the sample may reduce or totally destroy its superconductivity (Foner and Schwartz 1981).

The first laboratory attempt to produce Nb_3Sn wires was in 1961 at Bell Laboratories (Kunzler et al. 1961) by filling Nb tubes with crushed powders of Nb and Sn and drawing them into long wires. This primitive powder-in-tube (PIT) technique required reaction at very high temperatures, in the range of 1000–1400 °C, to form the superconducting Nb_3Sn phase. Nevertheless, that same year it was used to fabricate the first 6 T solenoid. An initial alternative to PIT wires and the first commercial production of Nb_3Sn were tape conductors fabricated by either chemical vapor deposition (1963) or by surface (or liquid solute) diffusion of Sn into a Nb

E. Barzi · A. V. Zlobin (✉)
Fermi National Accelerator Laboratory (FNAL), Batavia, IL, USA
e-mail: barzi@fnal.gov; zlobin@fnal.gov

D. Schoerling, A. V. Zlobin (eds.), *Nb_3Sn Accelerator Magnets*, Particle Acceleration and Detection, https://doi.org/10.1007/978-3-030-16118-7_2

This manuscript has been authored by Fermi Research Alliance, LLC under Contract No. DE-AC02-07CH11359 with the U.S. Department of Energy, Office of Science, Office of High Energy Physics.

substrate (1964). Although successful in demonstrating the use of Nb_3Sn in high-field magnets, none of these techniques were very practical. The large filaments in the case of the PIT wire, and the inherently large aspect ratio of the tape, invariably resulted in large trapped magnetization and flux jump instabilities.

A major step for practical Nb_3Sn production occurred with the discovery of the solid-state diffusion process. It was demonstrated in 1970 that the superconducting Nb_3Sn phase can be produced at the interface of Nb and a Cu-Sn alloy at lower temperatures compared to binary Nb and Sn couples. This principle allowed composite conductors to be formed in fine multifilamentary configurations by cold working, and before heat treatment. The bronze route (Howlett 1970; Kaufmann and Pickett 1971; Tachikawa 1971) was the first application of the above principles. To overcome the J_c limits of the bronze method the internal tin (IT) process was introduced in 1974 (Hashimoto and Yoshizaki 1974). The PIT, bronze, and IT methods were further developed into multifilamentary composites, and practically all commercially available wires are now produced by one of these methods.

In the 1980s and early 1990s, the development of Nb_3Sn conductor was mainly steered by fusion magnet programs. The Nb_3Sn toroidal magnetic system of the Tokamak T-15 was built and tested in the USSR at the end of 1988. The construction of the T-15 motivated the use of Nb_3Sn wires for the International Thermonuclear Experimental Reactor (ITER). The conductor-development programs for accelerator magnets were focused on Nb-Ti composite wires and were driven by the needs of accelerators such as the Tevatron, the Superconducting Super Collider (SSC), and the Large Hadron Collider (LHC). Since the late 1990s the high-energy physics (HEP) community has taken leadership in the development of Nb_3Sn wires for post-LHC accelerators to be used in high-field accelerator magnet research and development (R&D).

In this chapter we describe the development of commercial Nb_3Sn composite wires and tapes from the 1960s to the 1990s. We then illustrate the most important wire properties and their progress, as achieved in HEP by 2010. Finally, Rutherford cables are touched upon. These developments on wires and cables were crucial for the first reproducible accelerator-quality Nb_3Sn dipole and quadrupole magnets and their scale-up in the 2000s to the 2010s. Definitions of key wire and cable parameters are presented in Appendix 1. Properties and fabrication methods for Nb_3Sn composite wires and Rutherford cables have also been reviewed elsewhere (Dietderich and Godeke 2008; Bottura and Godeke 2012; Barzi and Zlobin 2016).

2.2 Development of Nb_3Sn from the 1960s to the 1990s

2.2.1 Nb_3Sn Development from the 1960s to the 1970s

The very first commercial Nb_3Sn composite conductor, which was used for accelerator magnet models in the period from the 1960s to the 1970s, was in the form of a flexible tape (also called a ribbon). A schematic of a Nb_3Sn ribbon is shown in Fig. 2.1.

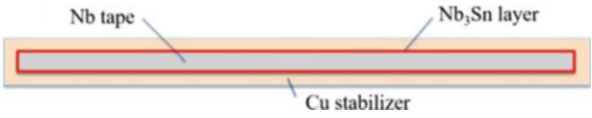

Fig. 2.1 Schematic of a cross-section of a Nb_3Sn ribbon

Tape conductors had been fabricated by chemical vapor deposition since 1963, and by surface diffusion of Sn into a Nb substrate since 1964. The latter process, also called Liquid Solute Diffusion, consisted of the introduction of a thin Nb tape into a molten Sn bath. The Sn-coated tape was then heated to ~1000 °C in a vacuum or inert atmosphere to form Nb_3Sn on both sides of the substrate. The tape was then Cu-cladded or Cu-plated for electrical stabilization. This technique was readily developed for long length production of ~500 m, and was first available in 1964 from the National Research Corporation in Massachusetts. Next, in 1965 the Compagnie Générale de Télégraphie sans Fil in France commercially produced a tape that was double the width and half the thickness, to allow for coil bending around smaller radii. In the same year, General Electric (GE) at Schenectady, NY, produced wide tapes with currents of 150 A, 300 A, and 600 A at 10 T. This was possible by fabricating tapes with a double substrate. GE also provided stainless-steel cladding, in addition to the Cu cladding option. And finally, in 1968 the Plessey Company in England introduced a diffusion-type Nb_3Sn narrow ribbon, which was Cu-cladded on one or both sides.

In parallel, chemical vapor deposition was developed, which is accomplished by hydrogen reduction of a mixture of chlorides of the constituent elements. By passing chloride over the metallic elements at ~1000 °C, gaseous chlorides such as $SnCl_2$ and $NbCl_4$ are produced. The chlorides are reduced by hydrogen and helium gasses, and the Sn and the Nb are deposited in the proper proportions onto substrates such as stainless steel. The A15 layer thickness was controlled by the rate at which the substrate was passed through the reaction chamber. Following deposition of Nb_3Sn, the ribbon was electroplated with a thin layer of nickel and then clad with silver or copper. The sole commercial producer of this material since 1963 had been the Radio Corporation of America (RCA), at Harrison, New Jersey, offering wide tape at current ratings of 300 A, 600 A, 900 A, and 1200 A at 10 T. It is to be noted that the vapor-deposited ribbon had a critical temperature of only 15 K, compared to 18 K for the diffusion process material. Whereas the commercial diffusion-type tapes were offered either bare or insulated with varnish, the vapor-deposited ribbon was just offered bare.

Conductor testing at that time included critical current and resistive critical temperature measurements of short samples, as well as continuous testing of the ribbon magnetization when passed through a 5 T field and measured with pick-up coils. This latter method produced the diamagnetic strength of the superconducting layer and allowed the detection of defects both in the superconductor and at the interface between superconductor and conducting metal. Unfortunately, information on the performance of these ribbons is limited. The best engineering current density of 500 A/mm^2 at 4.2 K and 12 T was obtained in a small-bore solenoid coil wound with RCA tape. The lowest current density of 270 A/mm^2 at 4.2 K and 2 T was seen in a 0.6 m long quadrupole with a large aperture.

It is interesting that, at that time, instabilities had already been recognized as a challenge. Ribbons had anisotropic properties and suffered from flux jumps in magnetic fields perpendicular to the tapes' wide face. In solenoidal coils, flux jump instabilities already occurred in magnetic fields below 8–10 T. Flux jumping was observed as voltage spikes much larger than expected by magnet inductance when ramping the current up and down. An experiment showed that by doubling the purity of the normal Cu conductor the current limits increased, but were still not at the short sample limit (SSL). When coils were instead used as inserts into a magnet and operated in background fields, the short sample limit was more likely to be achieved.

Requirements for superconductor stability with respect to magnetic flux jumps and superconductor protection in case of transition to the normal state led to the concept of composite superconducting wire, in which thin superconducting filaments are distributed in a normal low-resistance matrix. This matrix provides several important functions. It conducts heat away from the surface of the superconducting filaments because of high thermal conductivity, absorbs a substantial fraction of heat due to its high specific heat, and decreases Joule heating when the superconductor becomes normally conducting. To reduce eddy currents induced by varying external fields and improve the stability of composite wires to flux jumps, these filaments are twisted along the wire axis.

Multifilamentary Nb_3Sn composite wires were possible through the discovery of the solid-state diffusion process and by finding that Nb_3Sn can be produced at the interface of Nb and a Cu-Sn alloy at lower temperatures than for binary Nb-Sn couples. The formation of the brittle compound could be therefore postponed until the desired geometrical configurations for conductors (such as a multifilamentary wire) were achieved.

In the binary Nb-Sn system, single-phase Nb_3Sn is formed by solid-state diffusion above ~930 °C, where the only stable phase is Nb_3Sn. At temperatures below 845 °C, the two non-superconducting phases $NbSn_2$ and Nb_6Sn_5 are also stable, and all three phases will grow at the interface, with $NbSn_2$ most rapidly formed and Nb_3Sn being the slowest. In the ternary system (Nb-Cu-Sn), however, the only relevant stable phase is Nb_3Sn, even at lower temperatures. The diffusion path from the Cu-Sn solid solution to the Nb-Sn solid solution passes through the A15 phase field alone, preventing formation of the non-superconductive phases. In short, the addition of Cu strongly lowers the A15 formation temperature from well above 930 °C to practical values in industrial wires of ~650 °C, thereby also limiting grain growth and retaining a higher grain boundary density, as required for flux pinning.

This principle was used to fabricate multifilamentary Nb_3Sn composite wires by the so-called bronze route, which is still today one of the leading techniques for manufacturing Nb_3Sn wires for various applications. The bronze process is based on a large number of thin Nb filaments dispersed in a Sn-rich bronze matrix (Fig. 2.2).

The initial billet is made of hundreds of Nb rods, and it is drawn into a hexagonal element of intermediate size. The rods are then cut and assembled in a second billet, which is extruded, annealed, and drawn to the final wire size. The bronze core is surrounded by a high-purity Cu matrix that is separated by a thin Nb or Ta diffusion

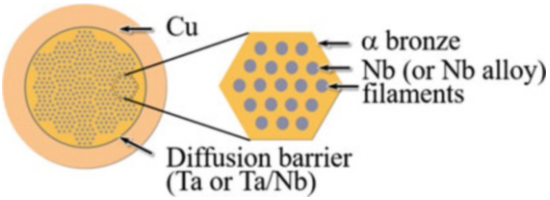

Fig. 2.2 Schematic of Nb_3Sn composite wire based on the bronze route. (Courtesy Peter Lee, FSU)

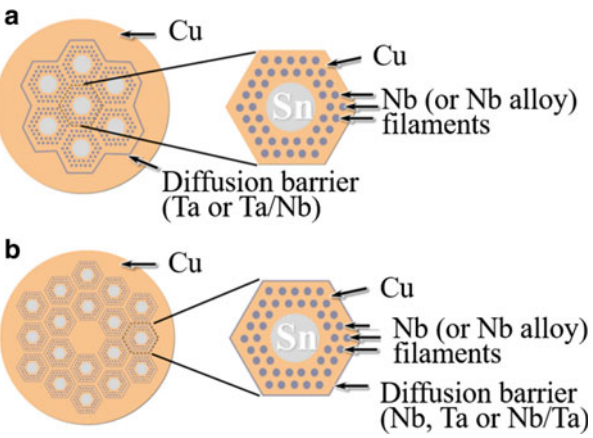

Fig. 2.3 Schematics of Nb_3Sn composite wire based on the IT process with: (**a**) single diffusion barrier; and (**b**) distributed diffusion barrier. (Courtesy Peter Lee, FSU)

barrier. The composite is twisted to increase electromagnetic stability and reduce AC losses. The bronze route provides the smallest filament size (~2–3 μm), but has a relatively low critical current density J_c due to the 13 wt% limited content of Sn in bronze.

The external diffusion process, a modification of the bronze method, was introduced in 1972. This process consists of extruding a Nb-Cu composite and drawing it to a final size. The wire is then coated with a layer of Sn before heating it to form a Cu-Sn alloy matrix and then Nb_3Sn filaments. The main benefit of this variant was that the Sn in the matrix was not limited as in the case of the bronze process. Its primary difficulty was delamination of the outer layer of the wire for plated Sn layers thicker than 5 μm. The maximum wire size was therefore limited to 0.25 mm.

The IT diffusion process, another modification of the bronze method, was first reported in 1974. This process consists of assembling Cu-clad Nb bars and a Cu-clad Sn-Cu alloy rod in a Cu tubing such that the Sn-Cu rod is at the center (Fig. 2.3). The assembly is then cold-drawn to final size. By restacking a number of assemblies and redrawing the billet down, a larger number of filaments and reduced bundle sizes are obtained. The advantage over the external diffusion process was that the Cu stabilizer, and a Ta barrier to protect the Cu from Sn diffusion, could be placed either outside of a wire in a single barrier configuration (Fig. 2.3a), or around each filament bundle in a distributed barrier configuration (Fig. 2.3b).

Another interesting method that was proposed in 1973 was the in situ process. It consisted of casting a Nb-Cu melt to form a dendritic network of Nb in Cu, and of drawing it to wire. Sn could be added in the initial melt or afterward before heat treatment. The most interesting aspect of this method was the great enhancement of the wire mechanical properties, due to the close proximity of the finely divided filaments.

Several companies were already active in producing commercial Nb_3Sn wires by that time. US companies included Airco, Inc., Intermagnetics General Corporation (IGC), Supercon, Inc., and Teledyne Wah Chang Albany (TWCA).

Airco, Inc. had started to manufacture superconductors in the mid-1960s at their Central Research and Development Laboratories in Murray Hill, NJ. They moved their manufacturing plant to Carteret, NJ in 1979. Their standard bronze wire was based on a modular approach, which meant combining one of three first extrusions containing 19, 55, and 187 rods, respectively, into second extrusion billets. In the 1970s Airco supplied 14 kg of 0.3 mm diameter 30% Nb in situ wire, Sn-plated on a commercial plating line in Airco's plant, to Brookhaven National Laboratory (BNL) for Nb_3Sn dipoles. In parallel, in cooperation with BNL, Airco developed a technique to wrap a multifilamentary Cu matrix conductor around a high-Sn Cu alloy core. The cable was then sheathed in Cu on a continuous tube mill to produce long lengths of finished wire. This was called the "distributed tin" process and reduced some of the problems encountered by external tinning. Airco also developed and brought to commercial maturity a high-rate magnetron sputtering process for producing Nb_3Sn tape for transmission lines by a variation of the bronze process.

In Europe, Siemens/Vacuumschmelze, Hanau, Germany, was producing bronze route wires on an industrial scale. Europa Metalli, LMI, Fornaci di Barga, Italy, and GEC Alstom Intermagnetics, Belfort, France, were producing IT wires.

In the USSR, the collaboration between the Kurchatov and Bochvar institutes and several plants of the nuclear industry focused on the development and production of Nb_3Sn wires for new thermonuclear facilities and for research magnets with high fields (Chernoplekov 1978). Studies of Nb_3Sn tapes were also conducted from 1962 to 1972. Equipment for the industrial production of tape by tinning was manufactured and installed in industry, but the work was stopped after the discovery of the solid-phase diffusion method. In 1972, intensive testing of multifilamentary samples based on Nb_3Sn composite wires began. The number of tests in subsequent years reached 3000 samples per year. These studies led to the Tokamak T-15 project with Nb_3Sn toroidal coils (Chernoplekov 1981). For this project, in the 1980s the USSR industry produced 30 tons of 1.5 mm diameter Nb_3Sn bronze wire with a Sn content of 10.5%.

Several Japanese companies also developed and produced Nb_3Sn composite wires. Sumitomo Electric Industries developed Nb_3Sn conductors in which the Nb_3Sn layer is formed by solid–liquid reaction between Nb tubes and the Cu-Sn alloy core (Yamasaki and Kimura 1982). This simpler method was later called the "internal-tin tube" or "tube-type" method. Mitsubishi Electric Co. was working on the internal Sn diffusion process, and Toshiba R&D Center and Showa Electric Wire and Cable Co. developed a Nb tube method. Furukawa Electric Company was working on bronze Nb_3Sn conductors with a large current capacity. Hitachi Ltd.

and Hitachi Cable Co. focused on large-scale multifilamentary Nb_3Sn composite wires.

By this time, critical current measurements of wires were performed within the bore of a solenoid on either straight samples a few centimeters long in a transverse field, or on a few turns wound around a 3.5–4 cm diameter barrel. The longer sample length allowed the use of a critical current criterion of 10^{-14} Ω m (i.e., smaller resulting voltages) as opposed to an electrical field criterion of 1 μV/cm. Inductive critical temperature measurements of short samples were sometimes added to conductor characterization as a means to identify lower critical temperature T_c regions in the material. The degradation of the critical current I_c due to the bending of the wire was measured as function of the bending diameter. The critical current density at 4.2 K and 12 T in the non-Cu samples ranged from 500 to 700 A/mm^2 in round wires.

2.2.2 *Nb_3Sn Development from the 1980s to the 1990s*

In 1980, TWCA proposed another innovative process called "jellyroll." In this process Nb foil was slit on a conventional slitter used to produce expanded mesh and rolled in a "jellyroll" together with bronze sheet. After wrapping with a diffusion barrier and a Cu stabilizer, the billet was compacted and then extruded and drawn in a conventional manner.

By the end of the 1990s, Oxford Superconducting Technology (OST), previously Airco, was fabricating Nb_3Sn multifilamentary wires with a modified jellyroll (MJR) process. In this version of the IT process, thin Nb sheets (with a thickness from 50 to 500 μm) were slit and expanded with controlled interconnection distances of 5–150 mm. The expanded Nb sheet (45–85% open) was then rolled up with the desired matrix material (i.e., bronze, Cu, Al, etc.) in the fashion of a jellyroll, inserted into a Cu container, sealed, extruded, and processed as conventional wire. A diffusion barrier was inserted if needed.

To overcome some of the constraints of the MJR process, OST also worked in the early 2000s on an internal Sn strand made with a restacking process called hot extruded rod (HER) process (Parrell et al. 2002). In this method, small Sn rods were inserted into the washed-out salt holes after extrusion. This technique, which was successfully demonstrated for a 37 restack, resulted in better bonding and had the potential for economic production of large quantities of conductor, as is the case for Nb-Ti. It was later abandoned, however, due to the relatively large effective filament diameter, or D_{eff}.

In September 1980, the Energy Research Foundation (ECN) from the Netherlands presented an alternative process that used both conventional and powder technologies. The core of a Nb tube was filled with fine grain size $NbSn_2$ powders inserted into a Cu tube and the resulting wire reacted at temperatures of 650–700 °C to form a continuous Nb_3Sn layer. The so-called PIT process was further optimized by the Shape Metal Innovation Company (SMI) (Lindenhovius et al. 1999) (Fig. 2.4).

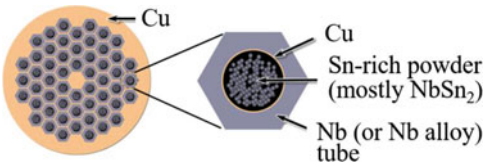

Fig. 2.4 Schematics of Nb_3Sn composite wire based on the powder-in-tube process. (Courtesy Peter Lee, FSU)

By the end of the 1990s, the strand samples used for I_c measurements were typically wound on grooved cylindrical Ti-alloy (Ti-6Al-4V) barrels, and held in place by two removable end rings. This method is still current today. After heat treatment, the Ti-alloy end rings are replaced by Cu rings, and voltage–current (V–I) characteristics are measured in boiling He at 4.2 K, in a transverse magnetic field provided by a solenoid. The voltage is measured along the sample by means of voltage taps placed 50 cm apart. The I_c is determined from the V–I curve by either the 10^{-14} Ω m resistivity or the 0.1 μV/cm electrical field criterion. The relative directions of the external magnetic field and the transport current are such as to generate an inward Lorentz force. Due to the latter and the differential thermal contraction between sample and barrel, the specimen is subject to a tensile strain of up to 0.05% at 12 T and 4.2 K. This strain leads to an overestimate of I_c between 3% and 5%. The n-values are determined in the $V(I_c)$-$10V(I_c)$ range by fitting the V–I curve with the power law $V \sim I^n$. Using this procedure, typical I_c uncertainties can be as low as ±1% at 4.2 K and 12 T, and about ±5% for the n-values. Magnetization measurements are performed with either balanced coil or vibrating-sample magnetometers.

Another new type of characterization included measuring the I_c of strands extracted from Rutherford-type cables. Plastic deformation during cabling affects the strand integrity. This phenomenon depends on the specific strand design and structure, and I_c degradation after cabling can be an indicator of internal damage.

2.3 Modern High-J_c Nb_3Sn Composite Wires

2.3.1 Target Parameters of Nb_3Sn Wires for HEP

IT and PIT are the two Nb_3Sn composite wire technologies, with sufficiently high J_c and availability in large quantities from industry, that were used in magnets for HEP applications in the new millennium. Commercial Nb_3Sn wires based on these two processes were further developed to meet the needs of accelerator magnets.

State-of-the-art PIT and IT wires benefited from at least two HEP-related conductor programs. The US Conductor Development Program (CDP) (Scanlan 2001) was started in 1999 by the US Department of Energy (DOE) as a collaborative effort of US industry, national laboratories, and universities with the goal of increasing the critical current density of Nb_3Sn IT wires for HEP applications including high-field accelerator magnets. Parallel R&D started in the early 2000s in the European Union as part of the Next European Dipole (NED) program (Devred et al. 2004). The target

Table 2.1 CDP, NED, and FCC Nb_3Sn wire target parameters

Parameter	CDP	NED	FCC
Non-Cu J_c (12 T, 4.2 K) (A/mm^2)	3000	–	–
Non-Cu J_c (15 T, 4.2 K) (A/mm^2)	–	1500	–
Non-Cu J_c (16 T, 4.2 K) (A/mm^2)	–	–	1500
Wire diameter (mm)	0.7–1.0	<1.25	1.0
Effective filament diameter D_{eff} (μm)	<40	<50	<50
Residual resistivity ratio RRR	–	>200	>150
Heat treatment time (h)	<200	–	–
Unit length (km)	>10	–	>5

parameters of Nb_3Sn wires for the superconductor R&D efforts of CDP and NED are summarized in Table 2.1.

Both programs had similar performance requirements in terms of J_c and D_{eff}, but NED was focused on the development of PIT composite Nb_3Sn wires of larger diameter (up to 1.25 mm) for high-field magnet applications. The effort was later continued by CERN with Bruker-EAS for the High Luminosity LHC (HL-LHC) upgrades.

Development of Nb_3Sn wires for high-field accelerator magnets continues. At present, properties are driven by the design studies of a Future Circular Collider (FCC) (Ballarino and Bottura 2015). The FCC Nb_3Sn wire specifications are also shown in Table 2.1. They are focused on reaching higher J_c at 16 T and on a significant reduction of conductor cost. The push for J_c increase is a stimulus for improving flux pinning using artificial pinning centers (APC) and increasing the upper critical field B_{c2} of Nb_3Sn. CERN is presently co-funding the R&D of several superconductor companies in Europe, Asia, and Russia to achieve the target parameters in commercial Nb_3Sn wires and to involve a sufficient number of companies in the longer-term production of large conductor volumes.

2.3.2 PIT Nb_3Sn Wires

The latest PIT process is based on stacking thick-wall round Nb tubes filled with fine $NbSn_2$ powder in a high-purity Cu matrix. The stacked assembly is drawn or extruded to the final wire size. This method allows an optimal combination of small filament size (<50 μm) and high J_c comparable with the IT process. The current cost of PIT wire is, however, a factor of two to three higher than the cost of IT wire.

The PIT process, first developed by the Netherlands Energy Research Foundation (ECN), was further optimized by the Shape Metal Innovation Company (SMI). In 2006 Bruker-EAS in Germany purchased the "know-how" for the PIT technology from SMI to industrialize this type of conductor. Cross-sections of some PIT composite wires produced by SMI and later by Bruker-EAS are shown in Fig. 2.5.

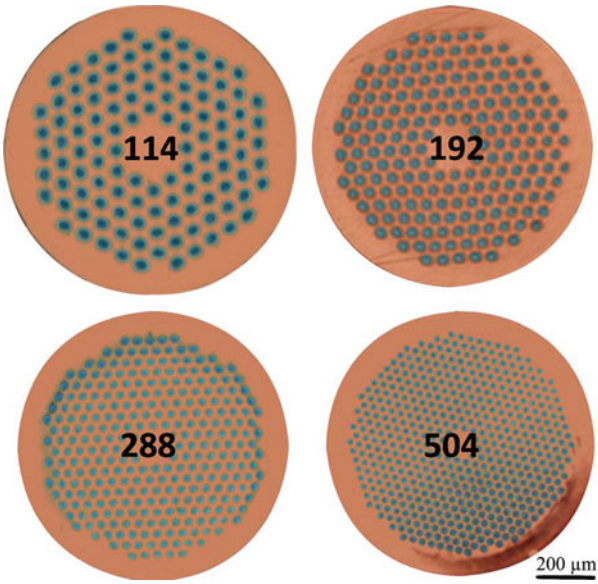

Fig. 2.5 Cross-sections of PIT wires of different designs (Courtesy of SMI and Bruker-EAS). The numbers represent the total number of superconducting tubes

The development of this technique has allowed the production of kilometer-long wires with 192 filaments. Shorter laboratory-scale wire samples with 504 and even 1332 filaments were also obtained. Wires were manufactured at Bruker-EAS in about 50 kg net production units. In 2008 the commercial PIT wire design started using round filaments instead of hexagonal ones to keep both the J_c and residual resistivity ratio (RRR) high during heat treatment and to reduce cabling degradation. These positive effects had been first demonstrated by SMI and Fermi National Accelerator Laboratory (FNAL) in 2004.

In PIT wires the Nb_3Sn A15 phase is formed in a solid-state diffusion reaction, typically after a few days at ~675 °C. The Sn diffusion and Nb_3Sn phase formation processes in the PIT route are described in detail elsewhere (Godeke et al. 2008). The $NbSn_2$ powder turns first into Nb_6Sn_5 and then into the Nb_3Sn phase. After 16 h, the initial Nb_6Sn_5 phase is converted into large grains. The void fraction in these regions is attributed to the reduced volume of Nb in Nb_3Sn, relative to the Nb_6Sn_5 phase. The Nb_3Sn phase formation ends after about 64 h at 675 °C, due to Sn depletion of the core–A15 interface region. Thus, a longer reaction does not increase the Nb_3Sn fraction. The outer boundary of the Nb_3Sn area is controlled to prevent Sn diffusion into the high-purity Cu matrix, and the resulting decrease in RRR. The heat treatment of commercial PIT composite wires without a diffusion barrier was optimized with respect to the area of reacted Nb to provide good RRR values. Most recently, PIT binary and ternary, mono and multi-filamentary wire configurations were successfully used at Hypertech Research Inc. to implement ZrO_2 precipitates as artificial pinning centers (APC) in the Nb_3Sn by means of internal oxidation of Nb-Zr.

2.3.3 IT Nb_3Sn Wires

As mentioned above, the IT process includes several versions, which differ, for example, in the design of the Nb filaments, the diffusion barrier position, the Sn distribution in the composite cross-section, sub-element and billet processing. Their potentials and limitations in terms of performance and large-scale production vary widely. IT composite wires were produced by several companies. In the USA, first IGC (Outokumpu since 2000, Luvata since 2005), and later OST (Bruker-OST since 2016) worked on this process. The Restack Rod Process® (RRP®), which was developed by OST in the early 2000s, provided the best results for accelerator magnet applications until February 2019, when short samples of APC PIT wires achieved the FCC J_c specifications shown in Table 2.1.

The IT RRP process is based on assembling a large number of Nb filaments and pure Sn or Sn-alloy rods in a Cu matrix (Parrell et al. 2004). The assembly is surrounded by a Nb barrier to prevent Sn diffusion into the high-purity Cu matrix, and it is then cold-drawn down to final size. Restacking of assemblies allows further reduction of the final sub-element size. Due to the fact that the diffusion barrier also reacts to form Nb_3Sn (and contributes to the J_c), there is a balance between sub-element size, metal ratios, heat treatment parameters, J_c, and Cu purity, which must be considered and optimized for every strand design.

During heat treatment of IT wires, several Cu-Sn phases are created and eliminated in the course of the Cu-Sn diffusion and Nb_3Sn formation processes. The presence of liquid phases in IT wires may cause motion of Nb filaments, allowing contact with adjacent ones; and the presence of voids may hinder the diffusion process. In addition, wire bursts can damage the wires. These problems were solved by using a three-step heat treatment cycle.

In the first step, temperature dwells below 227 °C allow the formation of a thin layer of a higher melting point Cu-Sn phase (ε-phase) that works as a container for the liquid Sn above 227 °C. A 1–3 day 210 °C dwell followed by 1–2 days at 400 °C provide appropriate Sn diffusion inside each sub-element, but also prevent Sn leaks through the Cu matrix, which is typically strongly deformed in the Rutherford cabling process. The superconducting Nb_3Sn phase is formed during the third step of the heat treatment cycle between 620 °C and 750 °C. During this stage the optimal phase microstructure, critical for flux pinning, is also formed. The Nb_3Sn microstructure is controlled by the temperature and the duration of this stage. Reactions at higher temperatures usually take the shortest time, but produce the largest grains. The choice of temperature and duration of the third stage is a compromise between an optimal pinning structure leading to high J_c, and Sn diffusion through the barrier leading to Cu pollution and to an increase of the matrix electrical and thermal resistivity.

Since 2002, when the RRP process was commercially introduced for HEP applications, OST has produced tons of Nb_3Sn wires. Cross-sections of some wire

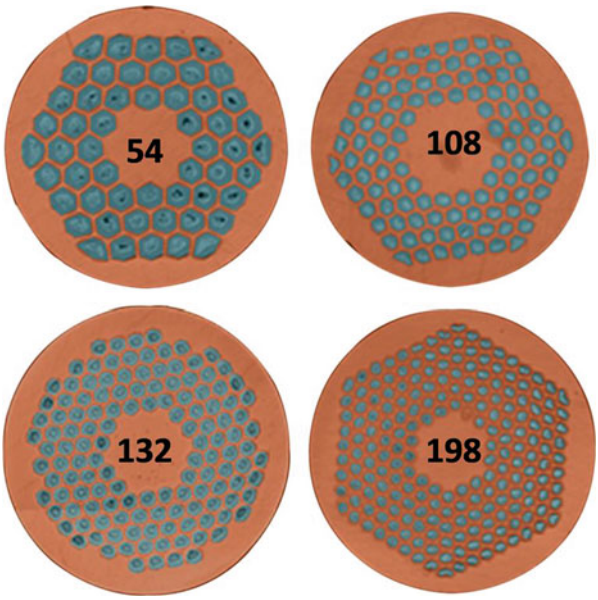

Fig. 2.6 Cross-sections of some commercial RRP wires (Courtesy of OST). The numbers represent the total number of superconducting sub-elements

designs manufactured by OST for accelerator magnets are shown in Fig. 2.6. In a configuration with 54 superconducting elements in a 61-restack wire (also represented as 54/61) of 0.8 mm size, the sub-element diameter is ~80 μm. Because of the impact of D_{eff} on conductor and magnet stability, OST focused on increasing the stack count in a billet to decrease the sub-element diameter.

As we will see below, in the Rutherford cables used in magnets, the Nb_3Sn filaments coalesced with each other. This "merging" randomly produced locally some superconducting areas several times larger than the size of the individual undeformed filaments (i.e., as in the round wire). These enlarged superconducting areas, which in cables may be up to five to six times the size of the undeformed filaments, clearly increase magnetic instabilities in cables. In 2006, OST produced for FNAL a 60/61 RRP billet with extra Cu spacing between sub-elements to reduce sub-element merging during cabling. Studies at FNAL showed that the mechanism by which the extra Cu thickness in the new OST design is effective is by providing a barrier to merging during reaction (i.e., not as much during the deformation process itself). Shortly afterward a 108/127 stack billet was produced with the same concept, and in 2007 OST adopted the spaced-filaments design as standard for HEP wires.

The 127-stack design entered production in 2008, with several tons utilized in HEP at 0.7–0.8 mm diameter and a D_{eff} of 45–52 μm. A third-generation wire with a 169-stack design followed in 2011. This wire has a D_{eff} of 40–58 μm for sizes of 0.7–1 mm. Integrated volume production of 169-stack RRP billets at OST is approaching that of the 127-stack billets. The development of 217-stack billets still continues.

Another improvement that OST obtained in RRP wires was that of interspersing Ti rods among the Nb filaments inside the sub-elements instead of using Ta-doped Nb filaments. This kind of doping allowed lowering the wire optimal reaction

temperatures from ~695 °C for Ta-doped wire to ~665 °C for a Ti-doped wire, thereby increasing the wire J_c at high fields, better preserving RRR, and also improving the irreversible strain limit (Cheggour et al. 2010).

In 2016, OST was purchased by Bruker, which recently stopped standard PIT production, making the RRP conductor a workhorse for Nb_3Sn accelerator magnets. Bruker continues to use the PIT technology in R&D as a possible platform for future high-J_c wires with APCs. Also, based on promising results in increasing the heat capacity of Nb_3Sn composite wires for improved stability (Xu et al. 2019), Bruker-OST is implementing hexagonal copper rods filled with mixed powder of rare earth oxides and copper in RRP re-stacks.

2.3.4 *Main Properties of Nb_3Sn Composite Wires*

2.3.4.1 Critical Current Density J_c and Critical Current I_c

The critical current density J_c is a key parameter, which controls the current-carrying capability, stability, magnetization, and AC losses of a superconducting wire, and thus the design field and performance of superconducting magnets. Improvement of the critical current density at 12 T and 4.2 K in commercial IT and PIT composite wires since 1980, when the best J_c for Nb_3Sn wires reached 0.5–0.7 kA/mm^2, is shown in Fig. 2.7.

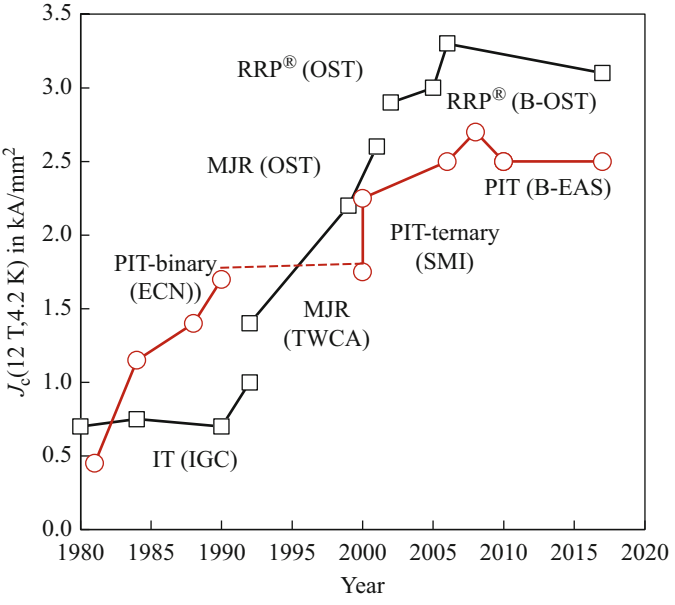

Fig. 2.7 J_c(12 T, 4.2 K) progress of IT and PIT composite wires

The J_c of PIT Nb_3Sn is affected by design parameters such as filament size, number of Nb tubes, use of binary Nb_3Sn or ternary $(NbTa)_3Sn$, and the quality and size of the $NbSn_2$ powder. During the 1980s the J_c of PIT wires was increased by ECN to 1.7 kA/mm^2 at 4.2 K and 12 T. The next step to ~2.3 kA/mm^2 was made by SMI in 2000. The maximum non-Cu J_c at 12 T and 4.2 K in PIT reached ~2.7 kA/mm^2 in 1.25 mm wires with 288 filaments of 50 μm, developed by SMI for the NED program. In the most recent composite wire, produced by Hypertech Research Inc. in 2019 using PIT technology and APC, the J_c in short samples approached to 1.5 kA/mm^2 at 16 T field, which corresponds to J_c of ~3.6 kA/mm^2 at 12 T. For commercial PIT wire production at Bruker-EAS, the J_c at 12 T and 4.2 K was ~2.5 kA/mm^2.

Optimization of the IT wire design and processing at OST from 1999 to 2006 produced fast progress in J_c at 12 T and 4.2 K, from ~1.5 kA/mm^2 to more than 3 kA/mm^2. The record J_c(12 T, 4.2 K) of 3.3 kA/mm^2 was achieved first in a RRP wire of 54/61 design and a diameter of 0.7 mm. The peak value of J_c(12 T, 4.2 K) in RRP wire production has been essentially stable since 2005. A J_c(12 T, 4.2 K) at or above 2.5 kA/mm^2 is routinely achieved in commercial wires.

The critical current density of Nb_3Sn is a function of magnetic field B, temperature T, and strain ε. Several empirical scaling laws were proposed to parameterize the J_c data (see Appendix 1). One of the practical purposes of parameterization is that of calculating the expected performance of a magnet from I_c measurements of strand samples used as witnesses during coil reaction. The intersection of the critical surface of each coil at the various magnet test temperatures with the B_{peak} load line of the magnet produces the expected coil SSL at that temperature. It is to be noted that SSL values for accelerator magnets typically have very little sensitivity (<0.3%) to the scaling law that is used.

Figure 2.8 shows an example of the critical current for a Nb_3Sn wire vs. magnetic field measured at 4.2 K. Measurements were performed by either current ramping in a fixed magnetic field (V–I method) or field ramping at a fixed transport current (V–H method). Closed symbols represent I_c data measured in a smooth

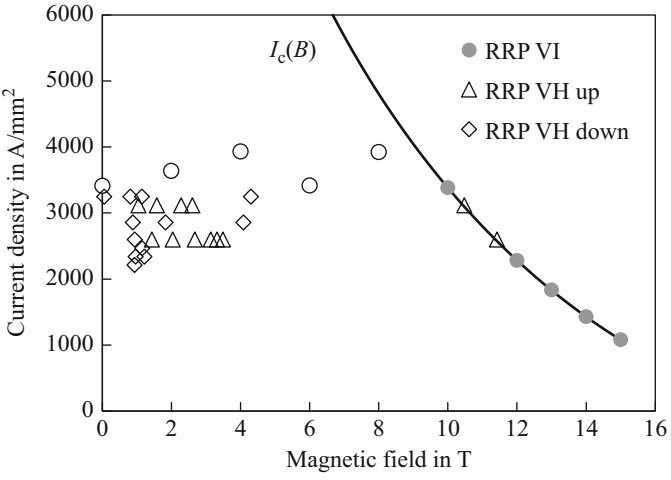

Fig. 2.8 Critical current of a Nb_3Sn wire vs. magnetic field measured at 4.2 K

voltage–current transition, whereas open symbols denote the maximum current I_q reached before a premature quench due to instabilities. An $I_c(B,T)$ parameterization curve is shown by the solid line.

2.3.4.2 Flux Jump Instabilities

Flux jumps in Nb_3Sn composite wires, predicted by stability criteria at fields below certain levels (Wilson 1983), are observed in critical current and magnetization measurements. In critical current measurements the flux jumps are recorded as large voltage spikes and premature quenches below the superconductor critical surface $I_c(B,T)$ during either *V–I* or *V–H* measurements. An example of flux jump instabilities in critical current measurements of RRP wires is shown in Fig. 2.8. In magnetization measurements they are seen as a sawtooth pattern at the low fields (Fig. 2.9). Flux jump instabilities may cause magnet premature quenches and also complicate quench detection in magnets.

2.3.4.3 Nb_3Sn Wire Magnetization

Magnetization of a composite wire plays an important role in superconducting accelerator magnets, which have demanding requirements on field uniformity. Magnetization loops measured at low field ramp rates ($dB/dt < 0.02$ T/s) for IT (IGC), RRP, and PIT wires are shown in Fig. 2.9 per non-Cu volume.

The magnetization of a composite superconducting wire has eddy current and hysteretic components (see Appendix 1). The eddy current component of magnetization in Nb_3Sn composite wires is suppressed by using a small wire twist pitch l_p. For $l_p < 15$ mm and a rather low matrix transverse resistivity $\rho \sim 10^{-10}\ \Omega$ m, the eddy current

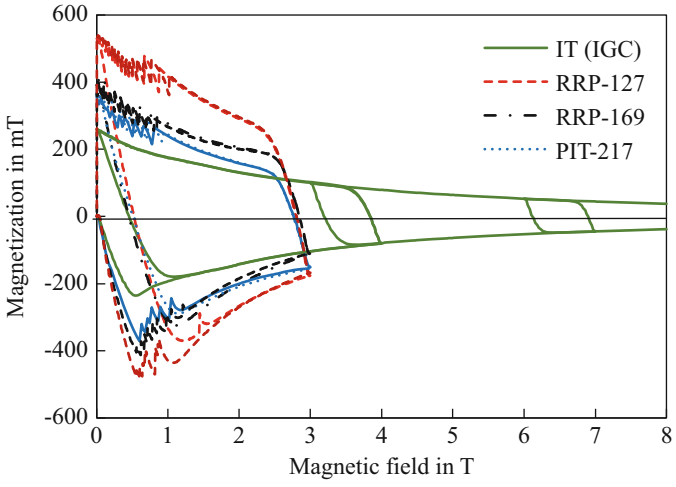

Fig. 2.9 Nb_3Sn wire magnetization per non-Cu volume

magnetization component is less than 1% of the hysteretic component at $dB/dt < 0.1$ T/s, which are typical maximum field variation rates in accelerator magnets.

As expected for the hysteretic component, the magnetization loop width is larger for wires with higher J_c and larger D_{eff}. Due to the larger J_c and D_{eff}, the level of wire magnetization as well as the range of wire re-magnetization when dB/dt changes sign are more than an order of magnitude larger than for Nb-Ti wires used in accelerator magnets. A large magnetization leads to field quality deterioration. Flux jumps also produce field fluctuations from cycle to cycle in accelerator magnets at low fields.

2.3.4.4 Cu Matrix RRR

RRR is a measure of Cu matrix purity, which is important for strand stabilization and magnet quench protection. It is defined as the ratio of the Cu matrix resistivity at room temperature R_{300} to its residual resistivity $R_{4.2}$ at $T = 4.2$ K. When measuring the RRR of the Nb_3Sn wire matrix, $T = 19$ K. A low RRR indicates damage of the internal structure of the strand and Sn leakage into the Cu matrix.

RRR depends on the type of Cu used, on the amount of Sn in the billet, on the diffusion barrier thickness, and on the heat treatment cycle. For instance, when using the same heat treatment cycle for IT wires, RRR values ranging from about 20, to 60, to 160 were obtained for barrier thicknesses of 3 μm, 4.2 μm, and 6 μm, respectively.

Typical RRR values for the latest PIT and RRP round wires are about 200 to 300. Bruker-OST uses Cu 101 with a RRR rating of 300 for a majority of their billets. To maintain a good RRR, OST had also been working on optimizing the Sn fraction in the billet, as well as the diffusion barrier thickness. It is to be noted, however, that RRR, using as numerator the Cu matrix resistivity value at room temperature and zero magnetic field, reduces because of the magnetoresistivity effect, i.e., its value strongly decreases with increasing magnetic field. The same can be expressed in a so-called reduced Kohler plot, where the normalized magnetoresistance increase is shown against the magnetic field multiplied by the resistance ratio at 294 K over 19 K.

The magnetoresistivity effect is stronger for a higher purity Cu matrix, thereby reducing the importance of high RRR at larger fields.

2.4 Rutherford Cables Based on PIT and RRP Wires

2.4.1 Cable Design and Fabrication

Accelerator magnets use high-current, multi-strand superconducting cables to reduce the number of turns in the coils, and thus magnet inductance. The Rutherford cable, developed at the Rutherford Appleton Laboratory (RAL) in the early 1970s (Gallagher-Daggit 1973), has played a crucial role in establishing Nb-Ti accelerator magnet technology due to its excellent mechanical, electrical and thermal properties.

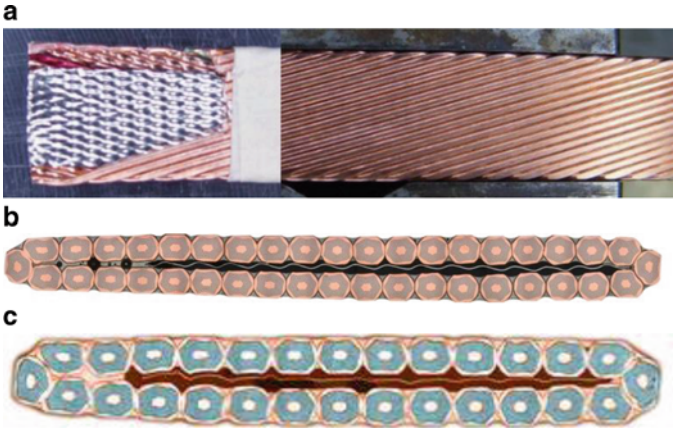

Fig. 2.10 Nb_3Sn Rutherford cables: (**a**) large face view of cable with stainless-steel (SS) core; (**b**) cross-sections of 40-strand cable; and (**c**) 28-strand cable with SS core

It is also widely used in Nb_3Sn magnets. Examples of Nb_3Sn Rutherford cables are shown in Fig. 2.10.

Rutherford cables are produced using special cabling machines, with single-pass and multi-pass approaches. In the former case, the cable is formed into its final cross-section in one single step, i.e., through the largest plastic deformation. In the multi-pass case, a cable with intermediate cross-sections with respect to its final geometry is produced first, which imparts plastic deformation more gradually. This method allows the use of an annealing heat treatment between cabling steps to release tension in the cable.

During cabling, quality monitoring includes checking for strand crossovers, when two adjacent strands alternate their position in the cable by crossing over each other during cable fabrication, and for sharp edges. Crossovers are deleterious to cable performance, and sharp edges are dangerous for the insulation, as shorts may be created. Cable width and thickness are measured periodically or continuously to keep their values within the required tolerances, which are usually of ± 6 μm for thickness and of ± 25 μm for width.

The Rutherford cable geometry is characterized by a cable aspect ratio, a geometrical cross-section area, a pitch angle, a packing factor (*PF*) and, if applicable, a keystone angle. Commonly used definitions of these parameters are summarized in Appendix 1. Large strand-plastic deformations, which were acceptable for a ductile superconductor like Nb-Ti, are not suitable for the more delicate Nb_3Sn strand structure. Examples of RRP strand cross-sections, as deformed after cabling, are shown in Fig. 2.11. Local sub-element deformations due to barrier breakage and merging are shown.

It was found that RRP and PIT strands behave differently under plastic deformation. Despite relative filament deformation being similar for the two, at increasing deformations RRP wires manifest some breaking, but also increasing merging between sub-elements, whereas PIT tubes show only some breaking under shearing.

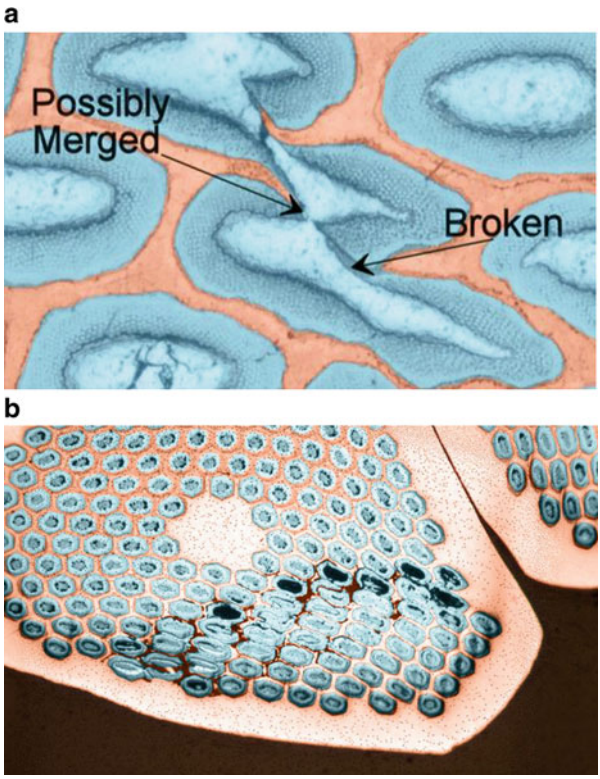

Fig. 2.11 Examples of: (**a**) a deformed RRP strand in a cable with local sub-element damage and merging; and (**b**) tube breakage in PIT wires

In both keystoned and rectangular cables the largest deformation values are found in the strands at the cable edges. The average strand deformation is lower in a less-compacted cable. Deformation of strand cross-sections in cables also causes deformation of the sub-elements, which depends on the cable packing factor *PF*.

The small edge deformation in Nb_3Sn keystoned cables should be larger than 0.85, and the width deformation should be slightly larger than 1.0, typically between 1.0 and 1.03, to avoid excessive strand deformation at the cable's thin edge. The limits on small edge deformation and cable width define a value for the optimal keystone angle of the cable cross-section.

The nominal cable *PF* for Nb_3Sn cables is within 84–87%. This *PF* range allows keeping the critical current degradation of Nb_3Sn Rutherford cables sufficiently low and at the same time provides adequate cable compaction to achieve the mechanical stability that is needed for coil winding.

2.4.2 Cable Size Changes after Reaction

A precise cable cross-section is important for achieving the required field quality in accelerator magnets. It is known that Nb-Sn composite strands expand after reaction

due to formation of the superconducting Nb_3Sn A15 phase. In round wires this expansion is isotropic. For Nb_3Sn Rutherford cables, however, an anisotropic volume increase was observed. It was found that the plastic deformation imparted during cabling releases itself through heat treatment, and therefore the thickness expansion is always larger than the width expansion. The volume expansion of a round wire increases with the Nb-Sn content, varying from 2 to 3% for both PIT and RRP wires.

The change in dimensions before and after reaction was measured for keystoned cables based on RRP strands. The average width expansion was 2.6%, the average mid-thickness expansion was 3.9%, and the average length decrease was 0.3%. Some cable samples were reacted under two different conditions, i.e., "unconfined" and "confined" in the transverse direction within a special fixture. The unconfined cable tests showed a clear longitudinal contraction by 0.1–0.2% for the cable made in two passes, and by 0.2–0.3% for the one-pass cable. The thickness and the width expansions in this case were 4% and 2%, respectively. When transversally confined to the unreacted cable cross-section, the cables elongated by ~0.4% and the thickness increased by only ~2%. The unconfined cables made of PIT strands with a Cu/non-Cu ratio of 1.2–1.3 showed a thickness expansion after reaction of 3–3.6% and a width expansion of ~1.5%. It was also reported that the cable width and thickness expansions were affected by the insulation. Braided insulation increased cable thickness expansion while simultaneously reducing the cable width expansion.

Cable thickness expansion after reaction is an important parameter for cables to be used in a magnet, and is therefore an important part of a magnet development plan. For magnetic design optimization, it is the reacted thickness and width values that are used as cable dimensions. The coil dimensions in the winding and curing tooling are determined by the unreacted cable cross-section, whereas the coil dimensions in the reaction and impregnation tooling are based on the reacted cross-section.

2.4.3 Cable Performance Parameters

The most important parameters that define the performance of a Rutherford cable in a magnet include the critical current I_c and average critical current density J_a, the Cu/non-Cu ratio, cable RRR, and interstrand resistances R_c and R_a, where R_c is the resistance between strands from the two cable layers and R_a is the resistance between adjacent strands within a layer. The parameters of the heat treatment cycle affect I_c, RRR, and contact resistances R_c and R_a.

2.4.3.1 Cable Critical Current I_c and Flux Jump Instabilities

The critical current I_c evaluation of Rutherford cables is performed by either testing short cable samples or individually extracted strands. The good correlation usually found between cable and extracted strand test results at high fields, as shown for instance in Fig. 2.12, confirms the validity of both approaches. As in Fig. 2.8, closed

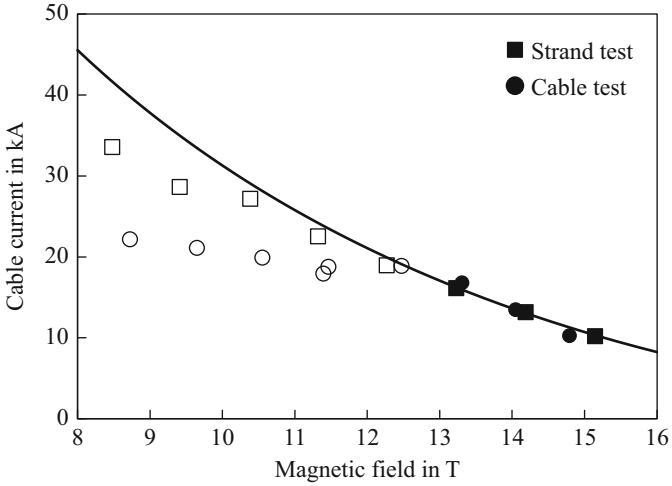

Fig. 2.12 Maximum current vs. magnetic field of a 40-strand Nb_3Sn cable with RRP strands. The solid line represents an $I_c(B)$ parameterization

symbols represent I_c data measured in a smooth voltage–current transition, whereas open symbols denote the maximum current I_q as reached before an abrupt quench due to instabilities. The solid line represents an $I_c(B)$ parameterization. A good correlation between extracted strand and cable test results also reveals a small variation of strand properties within the billets used in the cable, and is consistent with a uniform transport current distribution.

The effect of flux jump instabilities observed at low fields in Nb_3Sn wires was also seen in tests of short cable samples (see Fig. 2.12). Analysis and comparison of flux jump instabilities in Rutherford cables and their corresponding round wires show that these instabilities are larger in cables, due to sub-element deformation and possible sub-element merging (Fig. 2.11a), which in both cases lead to an increase of the local D_{eff}. The reduction of local RRR after cabling also increases flux jump instabilities in cables with respect to virgin wires.

2.4.3.2 Effect of Strand Plastic Deformation in Cables

Cable degradation studies and optimization are an important part of the magnet development process. The effect of cable plastic deformation on the critical current I_c, minimal stability current I_S and matrix RRR was studied using strands extracted from cables with different *PF*s. The results of I_c measurements made on extracted strands were compared with those made on the round wire from billets used in the cables. The cable I_c and critical current density J_a per cable cross-section area at 4.2 K and 12 T normalized to the I_{c0} and J_{a0} of a cable made of undeformed round strands ($PF = 78.5\%$), respectively, are plotted in Fig. 2.13 vs. cable *PF*. Whereas I_c

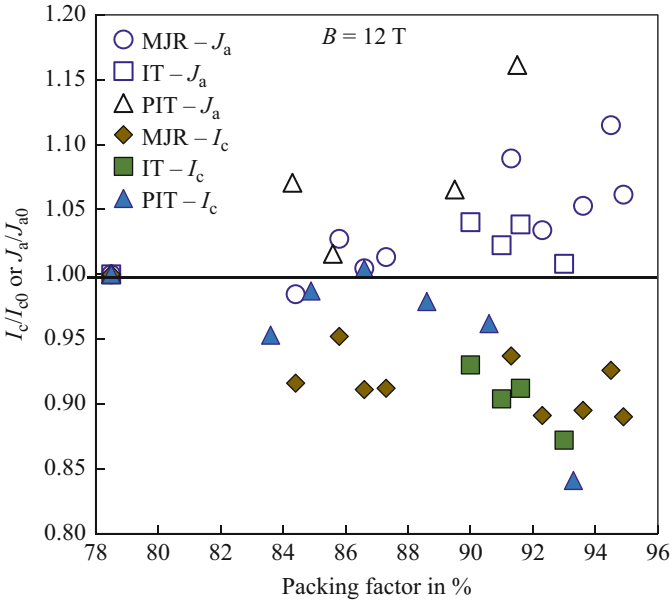

Fig. 2.13 Normalized cable I_c (filled markers) and J_a (unfilled markers) at 4.2 K and 12 T vs. *PF* for cables made with IT, MJR, and PIT Nb_3Sn strands

decreases with increasing *PF*, the normalized critical current density J_a in compacted cables is larger than in the undeformed cable, since the I_c degradation is less than the reduction of cable geometrical cross-section.

Some early IT wires demonstrated a relative I_c degradation of up to 80% at *PF*s above 84%. A large I_c degradation of up to 60% was also observed in early PIT strands. In 2004, however, SMI and FNAL found that by using round filaments in PIT wires, the I_c degradation could be reduced to 15% or less at *PF*s up to 94%. At a *PF* between 84% and 87%, which is typical for Nb_3Sn Rutherford cables, the I_c degradation in well-optimized cables is usually ~5% or less. Similar measurements performed at CERN on cables made with modern RRP and PIT strands are consistent with these data.

The effect of strand plastic deformation due to cabling on the stability current I_S and on the RRR is much stronger than on the I_c due to sub-element damage, and merging and Cu matrix contamination. It was also found that RRP strands with extra spacing between sub-elements were able to maintain a higher I_S in the higher *PF* range (above 90%).

Based on the results of I_c degradation in Nb_3Sn Rutherford cables, high *PF* values of 92–95% provide the highest J_a. Large I_S and RRR degradation values due to large deformations and possible damage and merging of the delicate sub-elements, however, impose an optimal *PF* within 84–87%.

2.4.3.3 Cable RRR

Due to the larger strand deformation at the cable edges, it was expected that RRR would vary along a strand. The first resistivity measurements made on extracted strands from high-edge compacted cables showed significant RRR degradation from an RRR $\approx$ 120 measured on strand segments on the cable faces. On the edges the results were an order of magnitude smaller, i.e., RRR $\approx$ 13, consistent with local Sn leakages through the diffusion barriers caused by the plastic deformation at the cable edges. Since this reduction is local, the average RRR value was still large, around 81. Such a large RRR degradation at the edges is often found even in cables with low packing factors. Recent measurements were performed at CERN on optimized cables made out of RRP132/169 wires with high RRR (between 100 and 250) for the 11 T dipole. The RRR reduction on the small edge was between 40% and 50%, and that on the large edge between 70% and 75% of the maximum values obtained on the cable flat parts.

2.4.3.4 Effect of Transverse Pressure

Transverse stress is the largest stress component in accelerator magnets, and can therefore damage brittle Nb_3Sn coils. To determine I_c sensitivity to transverse pressure, electro-mechanical tests are typically performed on either cables or encased wires. Transverse pressure studies are made by applying pressure to impregnated cable or wire samples and testing their transport current at several magnetic fields. Strain sensitivity, as previously indicated, increases with magnetic field. There are two components of the critical current degradation: a reversible component, which is fully recovered when removing the load, and an irreversible component. The latter is permanent. The irreversible limit is defined as the pressure leading to a 95% recovery of the initial I_c, or I_{c0}, after unloading the sample.

Institutions where transverse pressure measurements are performed include FNAL, the University of Twente, the National High Magnetic Field Laboratory, CERN, and the University of Genève. The I_c degradation strongly depends on conductor technology, but also on sample preparation and setup design. The former has an impact on possible stress concentration; the latter determines the sample's actual stress–strain state.

Figure 2.14 shows the total I_c degradation at 4.2 K and 12 T (unless otherwise indicated in figure caption), at transverse pressures up to ~200 MPa, of epoxy-impregnated Rutherford cables and encased wires made of PIT and RRP. Most of the load in this plot was applied cold. Older data (not shown) indicate that cables made of low-J_c strands are less sensitive to transverse pressure than those made with state-of-the-art, high-J_c strands. In some cases a stainless-steel core inside the cable also reduced pressure sensitivity.

In reference to magnet assembly and operation, it is important to distinguish the areas with maximum stress from those with maximum field, as well as the actual temperature conditions of the load application. Recent experiments performed at

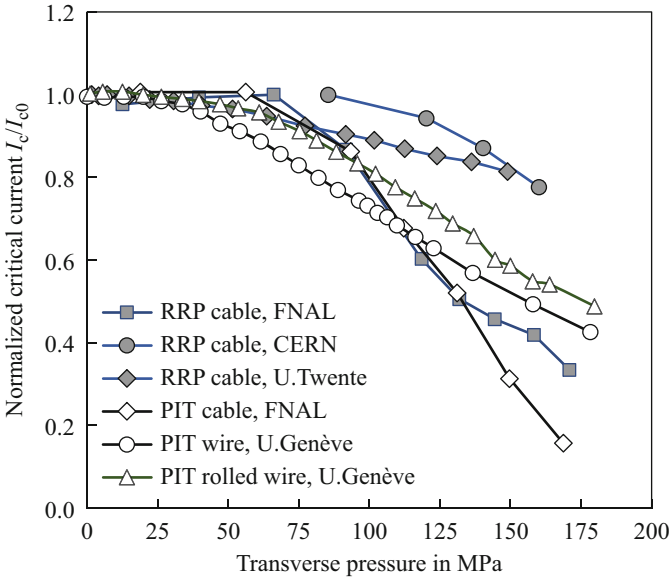

Fig. 2.14 Normalized I_c at 4.2 K vs. transverse pressure on Rutherford cable face or on encased wire for epoxy impregnated samples. All the Ic data correspond to 12 T, except for the PIT round and rolled wires which were measured by U. Genève at 19 T

FRESCA to measure the irreversible component with the load applied warm showed that the irreversible component is negligible at least up to 150 MPa. It is important that these studies continue.

2.4.3.5 Interstrand Resistance

Contact resistances between adjacent strands inside each layer, R_a, and between strands from different layers, R_c, control eddy current magnetization and AC losses, as well as current and heat sharing between strands in a Rutherford cable. To reduce eddy current effects without compromising cable electrical stability, one needs to increase R_c while keeping R_a low. Calculations show that for field ramp rates up to 0.1 T/s, R_c has to be larger than ~10 μΩ, and R_a larger than ~0.1 μΩ. In this case, the eddy current effect will be negligible with respect to the persistent current effect.

Direct measurements of R_c and R_a contact resistances performed under transverse pressures of 10–100 MPa gave $R_c = 1.1–1.4$ μΩ and $R_a = 8–16$ μΩ for Nb_3Sn cables without a core, and $R_c = 150–275$ μΩ and $R_a = 1.5–1.9$ μΩ for cables with a 25 μm stainless-steel core. Very low R_c values of ~0.1–0.4 μΩ were measured in Nb_3Sn Rutherford cables without a core reacted in coils under pressure. In cables with a full-width stainless-steel core, a high R_c of 246 μΩ was found based on AC loss measurements. For comparison, in the LHC Nb-Ti cables, typical R_c values under pressure are ~20 μΩ, i.e., an order of magnitude larger than in a Nb_3Sn cable without a resistive core, and an order of magnitude lower than in a Nb_3Sn cable with resistive core. Typical R_a values for Nb-Ti cables are ~170 μΩ.

Since the R_a limit is much smaller than the actual R_a data, their large variations will not affect magnet field quality or AC losses, whereas low values and large variations of R_c data in cables without a core will produce a large impact on magnet field quality and quench performance. Studies of interstrand contact resistances in Nb_3Sn Rutherford cables have shown that using a stainless-steel core is very efficient in reducing the level of eddy current effects (magnetization, AC loss) in cables. This approach is simpler than using a resistive coating, such as chromium, on individual strands. Resistive coating increases both R_c and R_a to 100 μΩ and higher, and may negatively impact the cable's electrical stability.

2.5 Conclusion

High-performance composite wires and Rutherford cables are key components of superconducting accelerator magnets. Whereas Nb-Ti has been the workhorse for HEP applications for almost 50 years, in the past 25 years Nb_3Sn wires and cables have made steady progress in wire fabrication techniques, understanding of their properties, and large-scale commercial production. They have now approached the necessary maturity to be used in accelerator magnets. Coupled with innovative development in the Nb_3Sn magnet technology itself, conductor progress has made it possible for accelerator magnets to achieve magnetic fields above 10 T, which is beyond the reach of Nb-Ti technology. In 2010, Nb_3Sn was adopted as the baseline conductor for the HL-LHC at CERN. Still, the potential of Nb_3Sn wires and cables is not fully apprehended. Work on Nb_3Sn composite wires for accelerator magnets continues, focusing on a better understanding and optimization of their technical performance and of their market parameters.

Appendix 1—Wire and Cable Parameterizations

The Rutherford cable geometry is characterized by a cable aspect ratio α and a cross-sectional area S_{cbl}, keystone and pitch angles, and cable packing factor *PF*.

Cable Aspect Ratio

The cable aspect ratio is the ratio of the cable width w to its mean thickness t

$$\alpha = w/t.$$

Cable Cross-Section

The cable cross-section is defined as the cable cross-section envelope

$$S_{\mathrm{cbl}} = w \cdot t.$$

Pitch or Transposition Angle θ

The cable pitch angle affects the cable's mechanical stability and the critical current degradation. Typical values of pitch angle in Nb-Ti cables used in accelerator magnets were within 13° to 17°. A study of the possible pitch angle range for Nb_3Sn Rutherford cables was performed using 1 mm and 0.7 mm non-annealed A101Cu strands. For 1 mm strands, below 12° the cable showed mechanical instability, and for angles larger than 16°, popped strands, sharp edges, and cross-overs occur. For 0.7 mm strands, the stable range of transposition angles was between 9° and 16°.

Cable Packing Factor PF

The cable packing factor, *PF*, is defined as the ratio of the total cross-section of the strands to the cable cross-section envelope $S_{\mathrm{cbl}} = w{\cdot}t$

$$PF \cong \frac{\pi N \cdot D^2}{4(w \cdot t - A_{\mathrm{core}}) \cdot \cos\theta},$$

where N is the number of strands in the cable, D is the strand diameter, w and t are the average cable width and thickness, θ is the cable transposition angle, and A_{core} is the cross-sectional area of the core.

The minimal *PF* for a Rutherford cable, i.e., one having a non-deformed cross-section, has a value of $\sim\pi/4 = 0.785$. To provide cable mechanical stability and precise width and thickness (parameters that are important for accelerator magnet coils), Rutherford cables are usually compacted by compressing their cross-section in both transverse directions. For an I_c degradation limited to 5–10%, increasing the cable *PF* also allows raising the cable average current density J_a, which is defined as

$$J_a = I_c / S_{\mathrm{cbl}}.$$

Cable Edge and Width Deformations R_e, R_w

The critical current degradation is determined mainly by the amount of cable cross-section deformation. The deformations of cable edge R_e and width R_w are defined as

$$R_e = \frac{t}{2D},$$
$$R_w \cong \frac{2w \cdot \cos\theta}{N \cdot D},$$

where D is the strand diameter, N is the number of strands in the cable ($N = N + 1$ in the case of odd N), and θ is the cable transposition angle. They can also be expressed as edge c_t and width c_w compactions (Bottura and Godeke 2012), which are related to R_e and R_w as

$$c_t = R_e - 1,$$
$$c_w = R_w.$$

Critical Current Density

Critical current density is a key parameter, which controls the current carrying capability, stability, magnetization, and AC losses of a superconducting wire, and thus the performance of superconducting magnets. Parameterizations of the critical current density as a function of magnetic field B, temperature T and strain ε, can be generally expressed as

$$J_c(B,T,\varepsilon) = \frac{C(t,\varepsilon)}{B}(1-t^m)^n b^p (1-b)^q,$$

where

$$b = B/B^*_{c2}(T,\varepsilon),$$
$$t = T/T_{c0}(\varepsilon),$$
$$B^*_{c2}(T,\varepsilon) = B^*_{c20}(0,\varepsilon)(1-t^\nu)k(t).$$

Parameters m, n, p, q, and ν as well as functions $C(t,\varepsilon)$, $T_{c0}(\varepsilon)$, $k(t)$, and $B^*_{c20}(0,\varepsilon)$ are usually determined by fitting experimental data of Nb_3Sn wires. For the practical strain range of $-1 < \varepsilon < 0.5$, the experimental data are well fitted with $m = n = q = 2$, $p = 0.5$, $\nu = 1.7$–2, and $C(t,\varepsilon) = C(\varepsilon)$.

Engineering Current Density

The engineering current density J_E is defined as the critical current density per total conductor cross-section. It depends on the superconductor J_c and superconductor fraction in the composite cross-section

$$\lambda = 1/(1 + r),$$

where r is the Cu/non-Cu ratio.

Magnetization and AC Losses

A composite superconductor placed in a varying magnetic field becomes magnetized (Wilson 1983) with a magnetization described by

$$M\left(B, \dot{B}\right) = -\mu_0 \left[\frac{2}{3\pi}\lambda J_c(B) D_{\text{eff}} + \frac{l_p^2 \dot{B}}{4\pi^2 \rho(B)}\right],$$

where D_{eff} is the effective filament diameter, l_p is the filament twist pitch, $\rho(B)$ is the effective transverse resistivity of the matrix, and $J_c(B)$ is the critical current density in the superconductor. The first term represents the component related to persistent currents in the superconducting filaments, and the second term represents the component associated with coupling eddy currents between filaments. Both components are diamagnetic in an increasing field and paramagnetic in a decreasing field. Composite wire magnetization plays an important role in superconducting accelerator magnets, which have demanding requirements on field uniformity.

Magnetic hysteresis leads to energy dissipation in superconducting composites (Wilson 1983). Similarly to magnetization, the power of AC losses P in a composite superconductor has two main components related to persistent and coupling eddy currents. The AC loss power per unit volume of composite wire after full flux penetration in the superconducting filaments can be represented as

$$P\left(B, \dot{B}\right) \cong \frac{2}{3\pi}\mu_0 \lambda J_c(B) D_{\text{eff}} \dot{B} + \frac{\mu_0 l_p^2 \dot{B}^2}{4\pi^2 \rho(B)}.$$

AC losses in composite superconductors play an important role in the thermal stabilization of superconducting coils during magnet operation and quench, and contribute to the heat load on a magnet cooling system.

Due to electromagnetic coupling between strands, the Rutherford cable magnetization and AC loss power include additional eddy current contributions, which depend on the cable geometry and interstrand contact resistances as

$$\vec{M}_c \cong -\mu_0 \left(\frac{8\alpha^2 L^2}{15\rho_c} \frac{d\vec{B}_\perp}{dt} + \frac{L^2}{3\rho_a} \frac{d\vec{B}_\perp}{dt} + \frac{L^2}{4\alpha^2 \rho_a} \frac{d\vec{B}_\parallel}{dt} \right),$$

$$P_c \cong \frac{8\alpha^2 L^2 \dot{B}_\perp^2}{15\rho_c} + \frac{L^2 \dot{B}_\perp^2}{3\rho_a} + \frac{L^2 \dot{B}_\parallel^2}{4\alpha^2 \rho_a},$$

where $4L$ is the cable transposition pitch, α is the cable aspect ratio, $B_\perp$ and $B_\parallel$ are the perpendicular and parallel components of the magnetic field to the cable wide surface, and ρ_c and ρ_a are the effective cable resistivity between cable layers and within a layer, respectively. The first term in both formulae provides the main contribution due to the large value of α. The parameters ρ_c and ρ_a are related to the measurable contact resistances R_c and R_a as

$$\rho_c = \frac{4\alpha L}{N^2} R_c \text{ and } \rho_a \cong \left(\frac{2L}{\cos\theta} \right)^2 R_a,$$

where R_c is the contact resistance of two crossing strands and R_a is the resistance per unit length of two adjacent strands in a cable.

References

Ballarino A, Bottura L (2015) Targets for R&D on Nb_3Sn conductor for high energy physics. IEEE Trans Appl Supercond 25(3):1–6. https://doi.org/10.1109/tasc.2015.2390149

Barzi E, Zlobin AV (2016) Research and development of Nb_3Sn wires and cables for high-field accelerator magnets. IEEE Trans Nucl Sci 63(2):783–803. https://doi.org/10.1109/tns.2015.2500440

Bottura L, Godeke A (2012) Superconducting materials and conductors, fabrication, and limiting parameters. In: Chao AW, Chou W (eds) Reviews of accelerator science and technology, vol 5. World Scientific, Singapore, pp 25–50

Cheggour N, Goodrich LF, Stauffer TC et al (2010) Influence of Ti and Ta doping on the irreversible strain limit of ternary Nb_3Sn superconducting wires made by the restacked-rod process. Supercond Sci Technol 23:052002. https://doi.org/10.1088/0953-2048/23/5/052002

Chernoplekov NA (1978) Superconducting magnet systems for plasma physics research in the USSR. In: Polak M et al (eds) Sixth international conference on magnet technology (MT-6), 29 Aug–2 Sep 1977. ALFA, Bratislava, pp 3–12

Chernoplekov NA (1981) Status and trends of SC magnets for thermonuclear research in the USSR. IEEE Trans Magn 17(5):2158–2167. https://doi.org/10.1109/tmag.1981.1061408

Devred A, Baynham DE, Bottura L et al (2004) High field accelerator magnet R&D in Europe. IEEE Trans Appl Supercond 14(2):339–344. https://doi.org/10.1109/tasc.2004.829121

Dietderich DR, Godeke A (2008) Nb_3Sn research and development in the USA—Wires and cables. Cryogenics 48(7–8):331–340. https://doi.org/10.1016/j.cryogenics.2008.05.004

Foner S, Schwartz BB (1981) Superconductor material science: metallurgy, fabrication, and applications. Plenum Press, New York

Gallagher-Daggit G (1973) Superconductor cables for pulsed dipole magnets. Technical report, Rutherford High Energy Laboratory Memorandum, No. RHEL/M/A25, Chilton, Didcot

Godeke A, den Ouden A, Nijhuis A et al (2008) State of the art powder-in-tube niobium–tin superconductors. Cryogenics 48(7–8):308–316. https://doi.org/10.1016/j.cryogenics.2008.04.003

Hashimoto Y, Yoshizaki K, Tanaka M (1974) Processing and properties of superconducting Nb_3Sn filamentary wires. In: Mendelssohn K (ed) Proceedings of the 5th international cryogenics engineering conference, 7–10 May 1974. Cryogenic Association of Japan/IPC Science and Technology Press, Guildford/Kyoto, pp 332–335

Howlett EW (1970) US Patent 3, 728, 165, 19 Oct 1970; UK Patent 52, 623/69, 27 Oct 1969

Kaufmann AR, Pickett JJ (1971) Multifilament Nb_3Sn superconducting wire. Bull Am Phys Soc 15:838. https://doi.org/10.1063/1.1659651

Kunzler JE, Buehler E, Hsu FSL et al (1961) Superconductivity in Nb_3Sn at high current density in a magnetic field of 88 kgauss. Phys Rev Lett 6(3):89. https://doi.org/10.1103/PhysRevLett.6.89

Lindenhovius JH, Hornsveld EM, den Ouden A et al (1999) Progress in the development of Nb_3Sn conductors based on the "powder in tube" method with finer filaments. IEEE Trans Appl Supercond 9(2):1451–1454. https://doi.org/10.1109/77.784664

Matthias BT, Geballe TH, Geller S et al (1954) Superconductivity of Nb_3Sn. Phys Rev 95(6):1435. https://doi.org/10.1103/physrev.95.1435

Parrell J, Zhang Y, Hentges RW et al (2002) Nb_3Sn strand development at Oxford Superconducting Technology. In: Balachandran B, Gubser D, Hartwig TK (eds) Advances in cryogenic engineering: proceedings of the international cryogenic materials conference, Madison, Wisconsin, 16–20 July 2001, Melville, vol 48. American Institute of Physics, New York, pp 968–977

Parrell JA, Field MB, Zhang Y et al (2004) Nb_3Sn conductor development for fusion and particle accelerator applications. Adv Cryo Eng (Materials) 50B:369–375. https://doi.org/10.1063/1.1774590854

Scanlan RM (2001) Conductor development for high energy physics-plans and status of the US program. IEEE Trans Appl Supercond 11(1):2150–2155. https://doi.org/10.1109/77.920283

Tachikawa K (1971) Studies on superconducting V_3Ga tapes. In: International cryogenics engineering conference Berlin, 25–27 May 1970. Iliffe Science and Technology Publications, Guildford, p 339

Wilson MN (1983) Superconducting magnets. Oxford University Press, New York

Xu X, Zlobin AV, Peng X, Li P (2019) Development and study of Nb_3Sn wires with high specific heat. IEEE Trans Appl Supercond 29(5):6000404

Yamasaki H, Kimura Y (1982) Fabrication of Nb_3Sn superconductors by the solid–liquid diffusion method using Sn rich CuSn alloy. Cryogenics 22(2):89–93. https://doi.org/10.1016/0011-2275(82)90100-x